Supplementary materials for

Disentangling the Hydrological and Hydraulic Controls on Streamflow Variability in E3SM V2 – A Case Study in the Pantanal Region

Donghui Xu[1*], Gautam Bisht[1], Zeli Tan[1], Chang Liao[1], Tian Zhou[1], Hong-Yi Li[2], L. Ruby Leung[1]

[1]Atmospheric Sciences and Global Change Division, Pacific Northwest National Laboratory, Richland, WA, USA
[2]Department of Civil and Environmental Engineering, University of Houston, Houston, Texas, USA

Correspondence to: Donghui Xu (donghui.xu@pnnl.gov)

Contents of this file

Text S1

Figure S1 to S7

Table S1

Text S1. Modified wetland inundation scheme

The functions of the surface water storage and outflow are determined by microtopography:

$$W_{sfc} = \frac{d}{2}\left(1 + \mathrm{erf}\left(\frac{d}{\sigma_{micro}\sqrt{2}}\right)\right) + \frac{\sigma_{micro}}{\sqrt{2\pi}}e^{\frac{-d^2}{2\sigma_{micro}^2}}, \qquad \text{Eq (S1)}$$

where W_{sfc} is the mass of the surface water $[kg \cdot m^{-2}]$, **erf** represents the error function, d is the height of the surface water relative to the cell averaged elevation $[m]$, and σ_{micro} is the standard deviation of the microtopographic distribution $[m]$, characterizing the sub-grid elevation variation. Since microtopography information is not available at large scale, the parameterization of σ_{micro} is proposed in Oleson et al. (2013):

$$\sigma_{micro} = \left(\beta + (\sigma_{max})^{\frac{1}{\eta}}\right)^{\eta}, \qquad \text{Eq (S2)}$$

where β is the topographic slope, σ_{max} represents the maximum value of σ_{micro}, and η is an adjustable parameter. The uncertainty of σ_{max} and η is not the focus of this study, hence, default values are accepted with $\sigma_{max} = 0.4$ and $\eta = -3$ (Oleson et al., 2013). Given the surface water height from previous equation, the inundation fraction (f_{h2osfc}) of the cell is estimated as:

$$f_{h2osfc} = \frac{1}{2}\left(1 + \mathrm{erf}\left(\frac{d}{\sigma_{micro}\sqrt{2}}\right)\right), \qquad \text{Eq (S3)}$$

The surface water storage functions as a linear reservoir when the f_{h2osfc} is larger than a threshold (f_c), and the outflow ($q_{out,h2osfc}$) is estimated as:

$$q_{out,h2osfc} = k_{h2osfc}f_{connected}(W_{sfc} - W_c)\frac{1}{\Delta t}, \qquad \text{Eq (S4)}$$

Where k_{h2osfc} represents the linear storage coefficient, W_c is the surface water mass corresponding the threshold fraction, Δt is the time step, and $f_{connected}$ is the fraction of connected inundated areas based on percolation theory:

$$f_{connected} = \left(f_{h2osfc} - f_c\right)^{\mu}, \qquad \text{Eq (S5)}$$

where μ is an exponent parameter. The values of f_c and μ are set to be 0.4 and 0.14 in default configuration, respectively.

We modified the wetland inundation scheme in ELM because the current scheme, by overestimating infiltration from the surface water storage, only produces trivial wetland inundation extent (Figure S1). In ELM, the simulated wetland inundation is controlled by surface-subsurface interaction (i.e., infiltration). Due to the typical coarse resolution of ESM simulation, sub-grid scale scheme is implemented to include the topography impacts on different processes. While a grid cell can be covered by different state variables (i.e., water, soil, snow),

the infiltration rate is constant across all the fractions (Figure S2). The infiltration capacity $(q_{infl,max})$ is formulated as:

$$q_{infl,max} = (1 - f_{sat})k_{sat}, \qquad \text{Eq (S6)}$$

where k_{sat} is the saturated hydraulic conductivity, and f_{sat} is the saturated area fraction, which is determined by the topographic characteristic and water table depth:

$$f_{sat} = f_{max}\exp\left(-0.5 \times f_{over} \times Z_{\nabla}\right), \qquad \text{Eq (S7)}$$

where f_{max} represents the maximum saturated fraction, and f_{over} is a decay factor $[m^{-1}]$. In the default ELM configuration, f_{over} is set to be 0.5 $[m^{-1}]$ for all grid cells.

　　The overestimation of infiltration in the surface water storage is a result of applying a uniform infiltration rate across landunits within each grid cell, although different fractions (standing water, open soil, etc.) are represented (Figure S2a). However, the infiltration under the surface water, where the water table is shallower and soil is more saturated, should be much smaller than open soil. Therefore, we developed a new sub-grid infiltration scheme to improve the simulation of wetland inundation in ELM (Figure S2). To constrain the infiltration from the surface water storage, it is reasonable to assume the saturation fraction overlaps with the surface water fraction instead of being uniformly distributed on different fractions (Figure S2). Specifically, we propose to estimate infiltration capacity on surface water fraction and other areas according to two potential situations (Figure S2):

$$\left. \begin{array}{l} q_{infil,max}^{h2osfc} = (1 - f_{sat})\Theta_{ice}k_{sat} \\ q_{infil,max} = \Theta_{ice}k_{sat} \end{array} \right\} , \quad f_{h2osfc} > f_{sat} \qquad \text{Eq (S8a)}$$

$$\left. \begin{array}{l} q_{infil,max}^{h2osfc} = 0 \\ q_{infil,max} = (1 - \dfrac{f_{sat} - f_{h2osfc}}{1 - f_{h2osfc}})\Theta_{ice}k_{sat} \end{array} \right\} , \quad f_{h2osfc} \leq f_{sat} \qquad \text{Eq S(8b)}$$

where $q_{infil,max}^{h2osfc}$ denotes the infiltration capacity in the surface water storage. The modified infiltration scheme significantly improves the simulation of wetland dynamics (Xu et al., 2023).
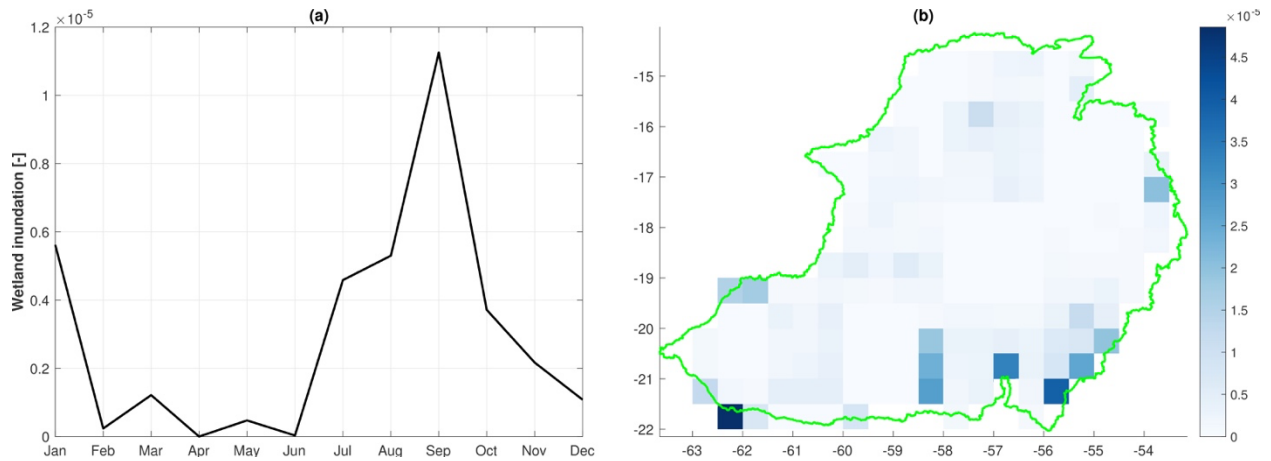
Figure S1. (a). Seasonality of simulated basin averaged wetland inundation fraction during 1979-2009. (b). Spatial pattern of annual averaged wetland inundation fraction simulation during 1979-2009.
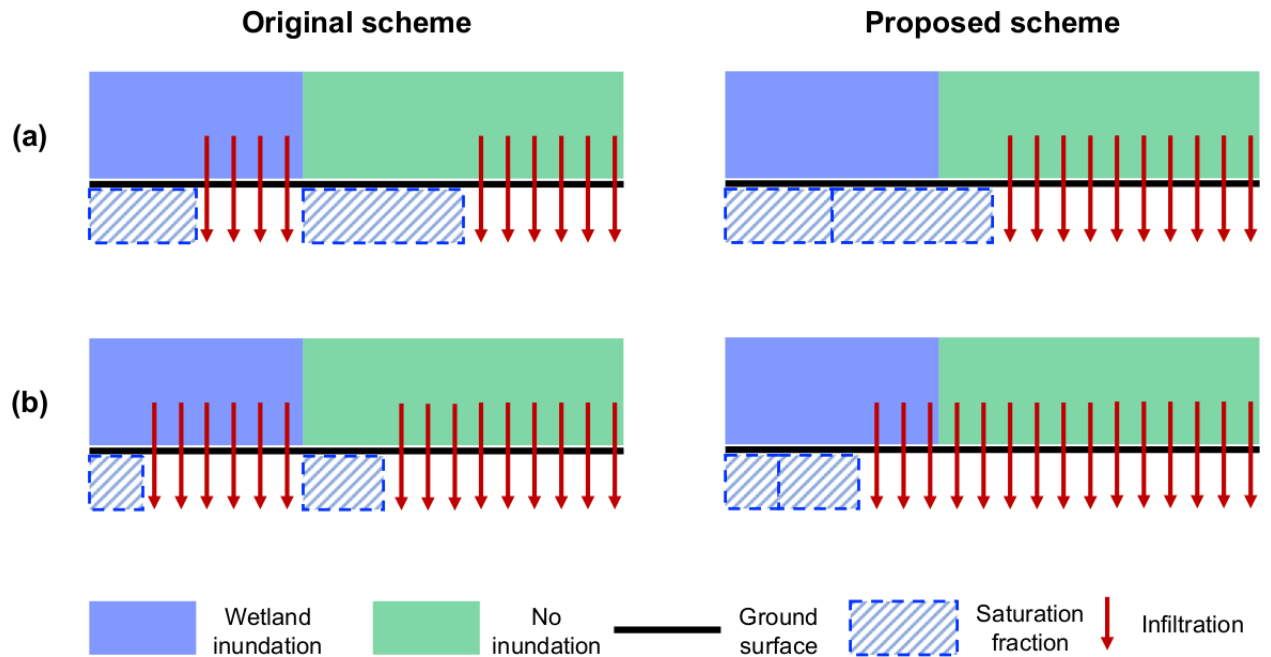

Figure S2. Sub-grid infiltration of the original scheme (left column), and proposed scheme (right column). Subplot (a) represents the situation that saturation fraction is larger than the wetland inundation, and subplot (b) represents the situation that saturation fraction is less than the wetland inundation.
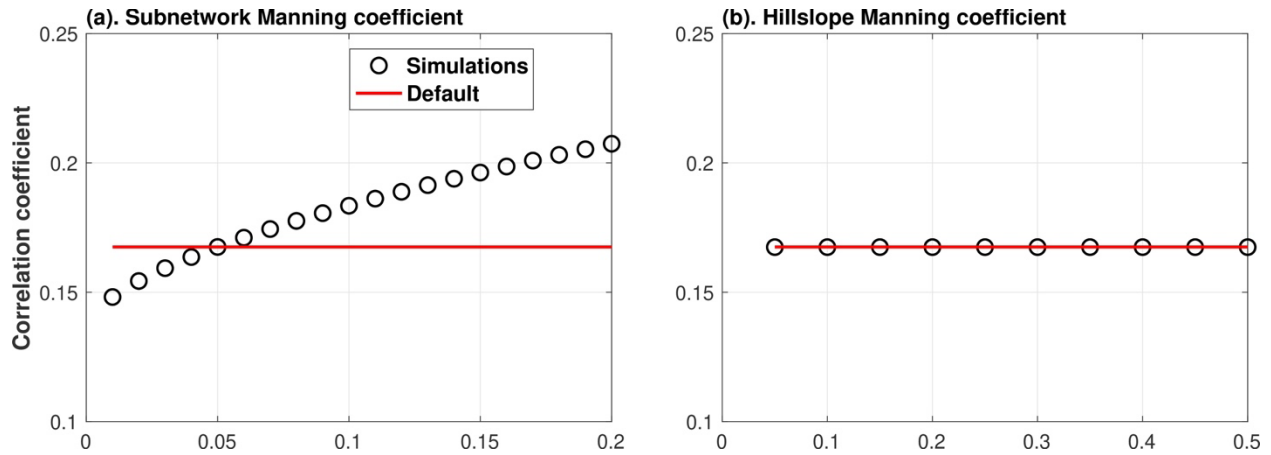
Figure S3. Sensitivity of (a). subnetwork Manning coefficient, and (b). hillslope Manning coefficient on simulated streamflow performance.
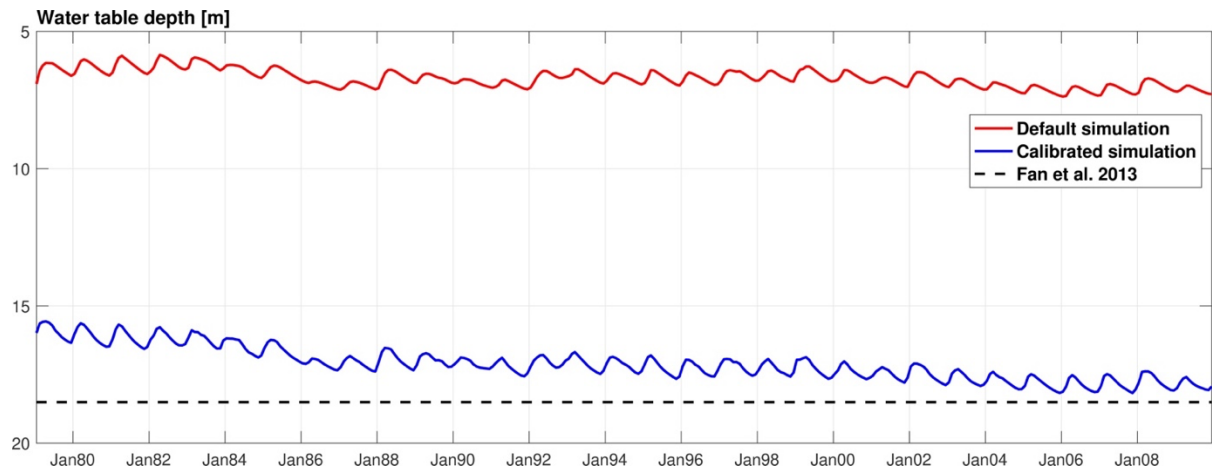

Figure S4. Basin averaged water table depth (WTD) comparison between simulations and dataset from Fan et al. (2013). Note, Fan et al. (2013) doesn't provide the time series of the WTD, therefore, the constant value is used to provide a reference for the magnitude of WTD.
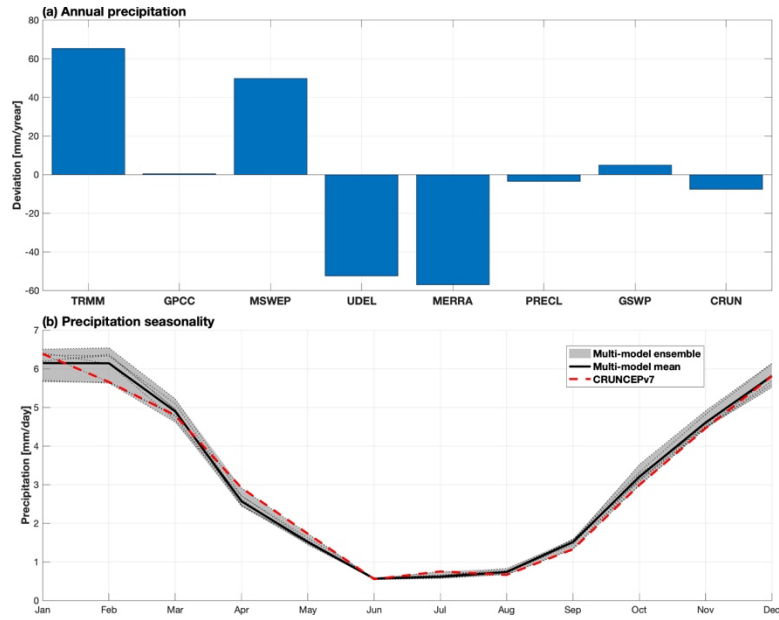
Figure S5. Precipitation uncertainty over upper Paraguay basin based on precipitation of 8 datasets.
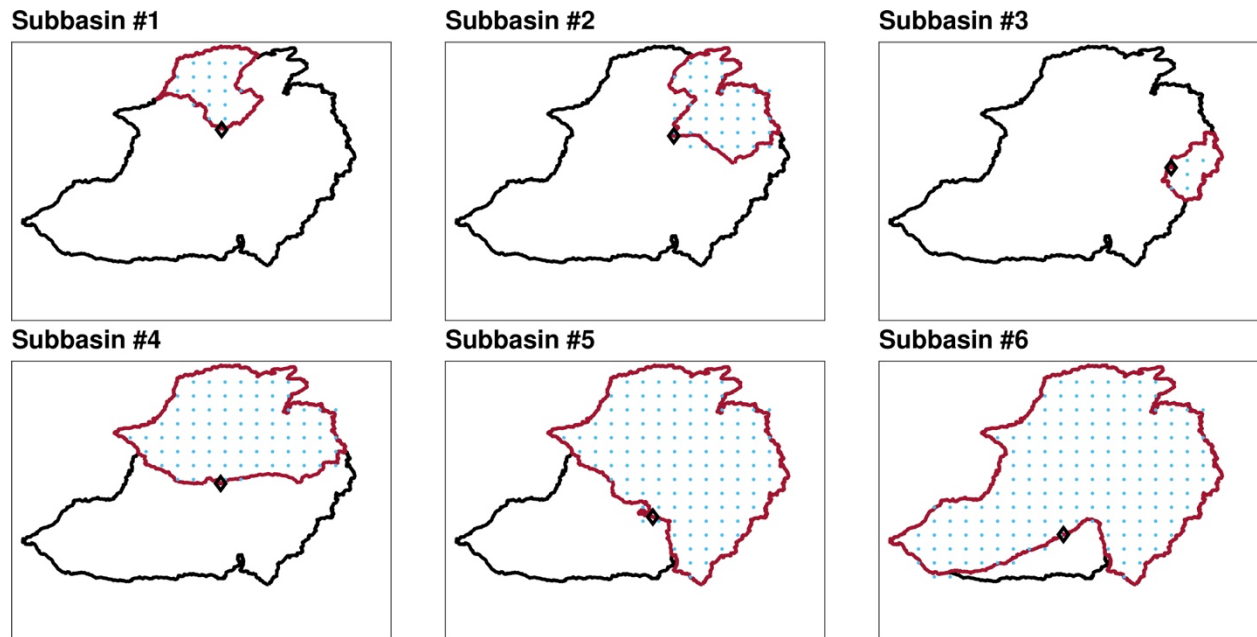

Figure S6. Top panel illustrates the location of the selected sub-basin gauges (black diamond) and corresponding water boundaries (red solid line). The blue dots are the grid cells that flow to the gauge in MOSART.
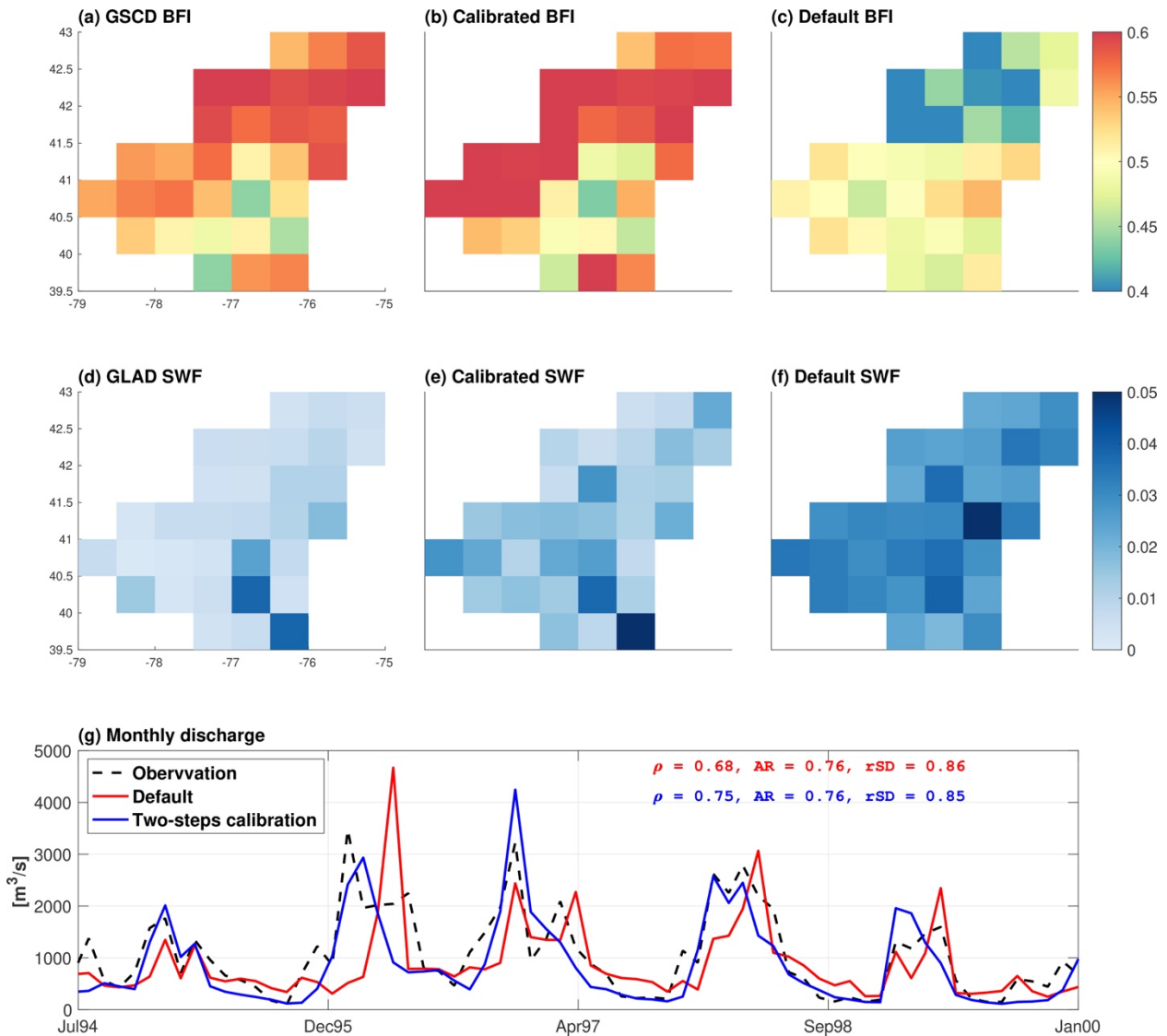
Figure S7. Evaluation of the two-step calibration over Susquehanna River basin. Only comparison between simulated streamflow and observed streamflow over 1994 to 2000 is shown in subplot (g), while the evaluation metrics were estimated based on the whole period (i.e., 1979 – 2010).

Table S1. Precipitation products used in this study

	Dataset	Spatial resolution	Temporal resolution	Availability
TRMM	The Tropical Rainfall Measuring Mission 3B43	0.25° × 0.25°	Monthly	1998-2019
GPCC	Global Precipitation Climatology Centre	0.5° × 0.5°	Monthly	1891-2016
MSWEP	Multi-Source Weighted-Ensemble Precipitation	0.1° × 0.1°	Monthly	1980-2019
UDEL	University of Delaware	0.5° × 0.5°	Monthly	1970-2017
MERRA	Modern-Era Retrospective analysis for Research and Applications	0.5° × 0.67°	Daily	1980-2015
PRECL	NOAA's Precipitation Reconstruction over Land	0.5° × 0.5°	Monthly	1948-2011
GSWP	Global Soil Wetness Project Phase 3 version 1	0.5° × 0.5°	3hourly	1901-2010
CRUN	CRUNCEP version 7	0.5° × 0.5°	6hourly	1901-2015